New Insights into the Dynamics of Concerted Proton Tunneling in Cyclic Water and Hydrogen Fluoride Clusters

Klaus R. Liedl,*,† Sanja Sekušak,‡ Romano T. Kroemer,§ and Bernd M. Rode†

Institute of General, Inorganic and Theoretical Chemistry, University of Innsbruck, Innrain 52a, A-6020 Innsbruck, Austria, Institute Rugjer Bošković, POB 1016, HR-10001 Zagreb, Croatia, and Physical and Theoretical Chemistry Laboratory, University of Oxford, South Parks Road, Oxford OX1 3QZ, England

Received: April 10, 1997[⊗]

The concerted proton transfer hypersurface of cyclic water and hydrogen fluoride clusters has been described by high-level molecular quantum mechanical calculations. For the cyclic water clusters the concerted proton transfer transition states have been investigated for the first time with methods including treatment of dynamic electron correlation. The crucial importance of dynamic electron correlation for the barrier heights is demonstrated. A detailed analysis of the minimum energy path has been performed. The reaction swath of the concerted proton transfer was examined indicating a reasonable description by harmonic approximation of the energy hypersurface. Transfer rates have been calculated by means of variational transition state theory with interpolated corrections (VTST-IC) and dual-level direct dynamics (DLDD), both with semiclassical tunneling corrections. Tunneling is very efficient in the concerted proton exchange reaction of the cyclic hydrogen-bonded clusters under investigation. Rate constants for the concerted exchange of hydrogens in important hydrogen fluoride vapor phase species are reported for the first time. In the hydrogen fluoride tetramer and pentamer the concerted proton exchange of four and five protons, respectively, takes place with reaction rates that are comparable with the concerted exchange rates in carboxylic acid dimers and is not hindered by the large number of simultanously moving protons. The concerted proton exchange rates in the studied water clusters are comparably low because of higher exchange barriers. It is shown that hydrogen fluoride clusters can be used to a large extent as "simplified" experimental and theoretical models for water clusters.

1. Introduction

Long-range proton transfer is a key step in many biological reactions.[1,2] In most of these reactions water plays a central role in the transfer of protons. Nevertheless, these proton transfer processes are not well understood mainly because of pronounced quantum effects in the nuclear motion of protons.[3] Several studies on charged or ionic water clusters have been published recently.[4,5,6,7,8] However, considering the autodissociation constant of water, it is quite clear that even at (locally) very low pH values nearly all the transporting agent is neutral, i.e., a major part of proton transfer processes has to be of "nonionic" nature. This implies that we need a better understanding of another concept that does not involve ionized species, namely, concerted proton tunneling, in order to explain the phenomenon of proton transfer completely. Whereas there is a deeper understanding of the ionic proton transfer, the models for concerted tunneling contributions are not well established. Most of the information available for concerted proton transitions arises from studies on carboxylic acid dimers.[9] The present study aims to improve the understanding of concerted proton transfer by giving a description of the hypersurface's shape as well as of the rate constants in small cyclic clusters of solvent molecules.

Cyclic clusters are optimal for concerted tunneling investigations, because it is possible to avoid the effect of ionic contributions completely and because they are approaching the description of the effects within an "infinitely" long chain because of their topology. The minimum energy structures of the cyclic water cluster have been investigated in numerous studies over the past years.[10−20] In 1992 Pugliano and Saykally[21] discussed the "clockwise and counterclockwise" tunneling motion that reverses the sense of the hydrogen bonding. To our knowledge, this concerted proton transfer has not yet been investigated in more detail after early pioneer studies[22] in 1991 yet.

Hydrogen fluoride clusters show similar effects but have several advantages concerning their investigation. First, the structural complexity of the clusters is significantly simplified because of their prevalent linear bond topology and their comparably high symmetry. This allows for an elucidation of certain characteristics of concerted tunneling proton transfer that might be less obvious in the corresponding water clusters. Not only are several effects less hidden in the structural simplicity of hydrogen fluoride clusters than in the complexity of the water clusters but also important effects are more pronounced, especially effects relying on cooperative many-body interactions.[23−32] It has been recognized that the hydrogen fluoride clusters of cyclic shape studied here are major components of hydrogen fluoride vapor.[24,29] Computational studies revealed astonishingly low barriers for concerted proton tunneling in cyclic hydrogen fluoride clusters.[33,25,34]

2. Methods

Recently, it has been shown that inclusion of dynamic electron correlation is necessary for a reasonable description of concerted proton transfer processes.[33,25,34] Therefore, all molecular quantum mechanical calculations in this study include an approximate

* To whom correspondence should be addressed.
† University of Innsbruck.
‡ Institute of Rudjer Boskovic.
§ University of Oxford.
⊗ Abstract published in *Advance ACS Abstracts,* June 15, 1997.

S1089-5639(97)01246-2 CCC: $14.00

TABLE 1: Energy Barriers [kcal/mol] (Values in Parentheses are Zero-Point Corrected)

	MP2	B3LYP
$(H_2O)_3$	27.0 (22.9)	26.3 (22.2)
$(H_2O)_4$	23.3 (16.9)	22.6 (16.3)
$(H_2O)_5$	26.1	25.0 (16.5)
$(HF)_3$	18.7 (16.0) [34]	16.6 (13.7) [36]
$(HF)_4$	12.7 (8.1) [34]	10.4 (6.0) [36]
$(HF)_5$	12.6[34] (6.5) [36]	9.8 (4.1) [36]

TABLE 2: Dynamic Electron Correlation Energy Difference $\Delta E_0^{(2)}$ between Minimum Energy Structures and Transition States [kcal/mol]

	$\Delta E_0^{(2)}$ (MP2)		$\Delta E_0^{(2)}$ (MP2)
$(H_2O)_3$	20.8	$(HF)_3$	16.8 [34]
$(H_2O)_4$	22.5	$(HF)_4$	15.9 [34]
$(H_2O)_5$	26.3	$(HF)_5$	17.0 [34]

treatment of dynamic electron calculation. Either this approximate treatment of dynamic electron correlation is performed by second order perturbation theory (frozen core MP2) or by the hybrid density functional method B3LYP.[35] Detailed investigations concerning the reliability of B3LYP for the description of hydrogen fluoride clusters showed that the hybrid density functional method is able to reproduce dynamic electron correlation effects predicted by second-order perturbation theory quite well, even though it cannot completely replace MP2 calculations.[36] Density functional theory benchmark studies for water clusters[13,37] led to similar conclusions.

If not otherwise denoted, all molecular quantum mechanical calculations were carried out using the 6-311++G(3df,3pd) basis set[38−40] with the Gaussian 94 series of programs.[41] The 6-311++G(3df,3pd) basis set was chosen because it offers higher angular momentum flexibility than the aug-cc-pVDZ[42−44] basis set at considerably lower computational demands than the aug-cc-pVTZ[42−44] basis set. For the calculation of stabilization energies of the clusters the aug-cc-pVDZ basis set is considered to be more advantageous because of the excellent convergence properties of MP2/aug-cc-pVxZ calculations in determining hydrogen bond strengths,[45,46,47] due to reduction of the so-called basis set superposition error or at least through a very reliable error compensation. However, in studying the concerted tunneling path and barriers, we assume the improvement of the monomers description by the basis functions of the other monomers within the complex to be rather constant and, therefore, to be more advantageous. These assumptions are confirmed by high-level benchmark calculations.[48] Hence, we consider the 6-311++G(3df,3pd) basis set as a good compromise between accuracy and affordable system size.

Reaction rate calculations were done with variational transition state theory with interpolated corrections (VTST-IC)[49] implemented in POLYRATE, version 6.5,[50] and dual-level direct dynamics (DLDD)[51] in MORATE version 6.5,[52] both with semiclassical tunneling corrections. (VTST-IC and DLDD are used as synonyms in the literature. However, we use the abbreviation VTST-IC when we relate to variational transition state theory based on interpolation between a comparably small number of high-level points. The approach relying on direct calculation of the energy surface at every point needed we will call DLDD in the following. This should not be confused with the interpolated corrections by means of the most accurate data available for minimum energy structures and transition states applied to both these methods.) These and related approaches developed by Truhlar and coworkers[53−58] have been tested successfully both against experiment[59−66] as well as against accurate quantum dynamics[67,68] and open the unique possibility of calculating reaction rates for systems with more than five atoms at an accuracy comparable to accurate quantum dynamical calculations.

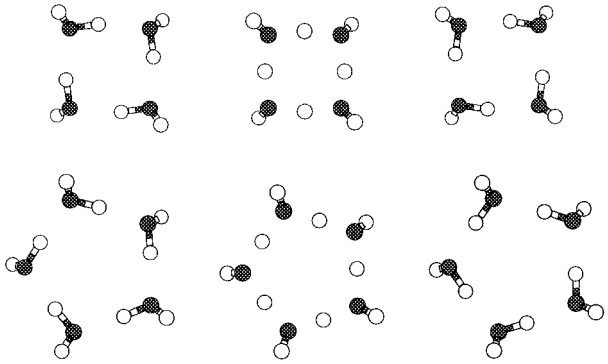

Figure 1. $(H_2O)_4$ and $(H_2O)_5$ concerted tunneling minimum energy structures and transition states.

3. Results

In the following sections 3.1, 3.2, and 3.3 we give a short overview of energetics, geometries and frequencies of both minimum energy structures and transition states followed by a detailed discussion of dynamics in section 3.4.

3.1. Energies. Table 1 contains the energy barriers for concerted proton transfer in cyclic water and hydrogen fluoride clusters. Details concerning the results for the hydrogen fluoride clusters are discussed elsewhere.[34,36] The excellent agreement of MP2 and B3LYP results regarding the barrier heights for the concerted proton transfer in cyclic water clusters is most striking. This excellent agreement is not due to smaller dynamic electron correlation contributions for water clusters in comparison to the hydrogen fluoride clusters as can be seen in Table 2. This table contains the dynamic electron correlation energy difference of minima and transition states at MP2 level of theory, i.e., $\Delta E_0^{(2)}$ in common terms of many-body perturbation theory.[69] As in the case of hydrogen fluoride, the neglect of dynamic electron correlation leads to a highly overestimated energy barrier. The better agreement between MP2 and B3LYP for water than for hydrogen fluoride is not a result of the lower demands for the description of dynamic electron correlation. It actually could arise from the parametrization procedure for B3LYP[35] that relies on more compounds with oxygen than with fluorine. It is also quite interesting that the concerted tunneling barrier of water seems to have its minimum at the tetramer whereas for hydrogen fluoride this seems to be the case for the pentamer.[25]

3.2. Geometries. Figure 1 displays the starting point, transition state, and end point of the concerted tunneling path for the water tetramer and pentamer. Whereas for hydrogen fluoride all minima have C_{nh} and all transition states have D_{nh} structures,[34] the situation for water is much more complicated as will be discussed below.

3.2.1. Minima. The minimum energy structures of cyclic water clusters in the gas phase are well known up to the hexamer.[10,11,15] The water trimer and pentamer are of C_1 symmetry whereas the tetramer is of S_4 symmetry. Tables 3−5 summarize the most important structural properties of the cyclic clusters minimum energy structures both for water and for hydrogen fluoride. The results for water agree quite well with results published so far. In the C_1 water structures we find O−O distances differing from each other. Generally, the O−O distance corresponding to the hydrogen bond with both "out-of-plane" hydrogens on one side of the "oxygen-plane" is the longest one and all others are close to the lower boundary given

TABLE 3: O−O and F−F Distances of Minimum Energy Structures [Å]

	MP2	B3LYP
$(H_2O)_3$	2.791−2.798	2.799−2.808
$(H_2O)_4$	2.731	2.741
$(H_2O)_5$	2.710−2.724	2.718−2.737
$(HF)_3$	2.613 [34]	2.593 [36]
$(HF)_4$	2.516 [34]	2.499 [36]
$(HF)_5$	2.484 [34]	2.467 [36]

TABLE 4: O−H and F−H Bond Distances of Minimum Energy Structures [Å] (Values in Parentheses Denote O−H Bond Distances of Hydrogens Not Taking Part in Hydrogen Bonds, i.e., the Ones of "Out-of-Plane" Hydrogens in the Water Clusters)

	MP2	B3LYP
$(H_2O)_3$	0.972 (0.958)	0.975 (0.960)
$(H_2O)_4$	0.979 (0.958)	0.983 (0.960)
$(H_2O)_5$	0.981 (0.958)	0.986 (0.960)
$(HF)_3$	0.933 [34]	0.942 [36]
$(HF)_4$	0.946 [34]	0.957 [36]
$(HF)_5$	0.950 [34]	0.963 [36]

TABLE 5: O−H and F−H Hydrogen Bond Distances of Minimum Energy Structures [Å]

	MP2	B3LYP
$(H_2O)_3$	1.897−1.919	1.902−1.925
$(H_2O)_4$	1.766	1.772
$(H_2O)_5$	1.730−1.748	1.734−1.754
$(HF)_3$	1.778 [34]	1.750 [36]
$(HF)_4$	1.591 [34]	1.563 [36]
$(HF)_5$	1.537 [34]	1.507 [36]

TABLE 6: O−O and F−F Distances of Transition States [Å]

	MP2	B3LYP
$(H_2O)_3$	2.367−2.370	2.379−2.381
$(H_2O)_4$	2.396	2.409
$(H_2O)_5$	2.396−2.398	2.411−2.413
$(HF)_3$	2.242 [34]	2.255 [36]
$(HF)_4$	2.265 [34]	2.280 [36]
$(HF)_5$	2.264 [34]	2.280 [36]

in Table 3. It could be that these differences in the O−O distances in the present study result from using default convergence criteria in the Gaussian 94[41] series of programs as suggested previously.[10,11] However, because the geometry optimizations were all started with identical O−O distances, the deviations of 0.01 Å for the trimer[15] and 0.02 Å for the pentamer do not appear to be artifacts.

In general, the F−F distances are considerably smaller than the corresponding O−O distances, indicating that the hydrogen bonds in hydrogen fluoride can profit more from forming cyclic clusters than those in water. However, the best available estimates for the noncyclic dimers[45,47] also show considerably larger O−O distances compared with F−F distances (2.91 and 2.73 Å, respectively).

The bond distances in Table 4 and the hydrogen bond distances in Table 5 have been listed for comparison with Table 7 of the following chapter.

3.2.2. Transition States. Tables 6 and 7 summarize the most important transition state geometry parameters. The water clusters transition state is of C_s symmetry for trimer and pentamer and of D_{2d} symmetry for the tetramer, whereas the transtion states of the hydrogen fluoride clusters are all of D_{nh} structure. The tendencies observed in changing from the minima to the transition states are the same for water and hydrogen fluoride. The most prominent feature is the decrease of O−O and F−F distances. However, this effect becomes smaller with

TABLE 7: O−H and F−H Distances of Transition States [Å] (Values in Parentheses Denote O−H Distances of Hydrogens Not Taking Part in Hydrogen Bonds)

	MP2	B3LYP
$(H_2O)_3$	1.213−1.216 (0.960)	1.221−1.223 (0.961)
$(H_2O)_4$	1.203 (0.959)	1.210 (0.960)
$(H_2O)_5$	1.196−1.202 (0.959)	1.203−1.209 (0.960)
$(HF)_3$	1.151 [34]	1.161 [36]
$(HF)_4$	1.138 [34]	1.147 [36]
$(HF)_5$	1.132 [34]	1.141 [36]

TABLE 8: O−H and F−H Stretching Frequencies of Minimum Energy Structures [cm^{-1}] (Values in Parentheses Denote O−H Stretching Frequencies Emerging from Hydrogens Not Taking Part in Hydrogen Bonds)

	MP2	B3LYP
$(H_2O)_3$	3628−3700 (3942−3946)	3542−3615 (3876−3881)
$(H_2O)_4$	3436−3574 (3937−3939)	3345−3484 (3874−3876)
$(H_2O)_5$		3287−3444 (3873−3879)
$(HF)_3$	3777−3893 [34,36]	3618−3749 [36]
$(HF)_4$	3418−3700 [34,36]	3197−3522 [36]
$(HF)_5$	3278−3612 [36]	3025−3419 [36]

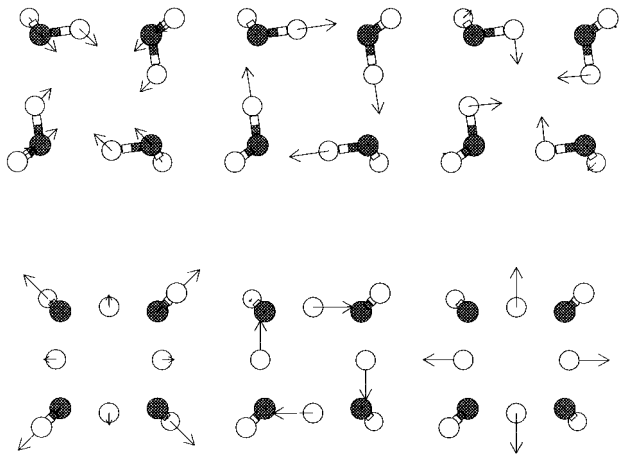

Figure 2. "Symmetric" O−O stretching, H−O stretching, and H−O bending modes of $(H_2O)_4$ minimum energy structure and transition state.

increasing cluster size. Within the C_s clusters O−O distance differences were found to be smaller than for the minimum structures and could even be regarded as insignificant within the limitations of the used convergence criteria.

3.3. Frequencies. For all minima and transition states except the water pentamer frequencies have been calculated at both MP2 and B3LYP levels. The water pentamer MP2 frequencies were computationalwise too expensive because of the low symmetry of this species. In the following only the frequencies corresponding to "symmetric" normal modes ("symmetric" H−O and H−F stretching, "symmetric" O−O and F−F stretching, and "symmetric" O−H and H−F bending), being the most relevant ones for concerted hydrogen exchange, are discussed. For the tetramer of water these "symmetric" modes are shown in Figure 2 for the minimum structure and the transition state. Detailed information concerning the water cluster minima frequencies and their assignment can be found in the literature.[11,18,15,20]

3.3.1. Minima. Table 8 gives an overview of the hydrogen stretching frequencies in the minima. The lower boundaries of the ranges given in Table 8 correspond to the "symmetric" bond stretching mode relevant for the concerted tunneling path.[34] As can be seen from stretching frequencies of "free" hydrogens, given in parentheses, the shift of water frequencies is reproduced quite well by B3LYP.

Tables 9 and 10 contain the remaining two "symmetric" modes, namely, the "symmetric" bending and the "symmetric"

TABLE 9: "Symmetric" O−H and F−H Bending Frequencies of Minimum Energy Structures [cm^{-1}]

	MP2	B3LYP
$(H_2O)_3$	875	893
$(H_2O)_4$	1011	1010
$(H_2O)_5$		1006
$(HF)_3$	973 [34]	1014 [36]
$(HF)_4$	1160 [34]	1197 [36]
$(HF)_5$	1179 [36]	1216 [36]

TABLE 10: "Symmetric" O−O and F−F Stretching Frequencies of Minimum Energy Structures [cm^{-1}]

	MP2	B3LYP
$(H_2O)_3$	217	216
$(H_2O)_4$	207	207
$(H_2O)_5$		179
$(HF)_3$	215 [34]	228 [36]
$(HF)_4$	210 [34]	224 [36]
$(HF)_5$	186 [36]	197 [36]

TABLE 11: "Symmetric" O−H and F−H Bending Frequencies of Transition States [cm^{-1}]

	MP2	B3LYP
$(H_2O)_3$	2028	2008
$(H_2O)_4$	1843	1813
$(H_2O)_5$		1699, 1799[a]
$(HF)_3$	2117 [34]	2059
$(HF)_4$	1835 [34]	1804
$(HF)_5$	1710	1674

[a] For the water pentamer there is a strong mixing of bending and "out-of-plane" modes preventing a strict assignment. Therefore, the two frequencies with the highest "symmetric" bending contribution are given.

O−O and F−F stretching modes. It is interesting to note the large similarity of the above-mentioned frequencies for water and hydrogen fluoride.

3.3.2. Transition States. Whereas the minimum energy structures and their frequencies are well-known in the literature, the concerted tunneling transition states for hydrogen fluoride have been investigated just recently in detail at a higher level of theory[34] and to our knowledge those for water have not been studied so far. This may be due to the conceptional difficulties of finding transition states between C_1 structures that involve the simultaneous cleavage of several bonds, even though the initial direction toward the concerted tunneling transition state—the direction of the "symmetric" O−O and F−F modes—always corresponds to the direction of an eigenvector with one of the five lowest eigenvalues of the minimum structures' mass-weighted matrix of second derivatives.

All transition states reported here are first-order transition states. The eigenvector corresponding to the "imaginary" frequency always points toward the concerted exchange of hydrogens, i.e. there is no indication for pathways toward ionic structures of the type $(H_3O)^+(OH)^-(H_2O)_{n-2}$ or $(H_2F)^+F^-(HF)_{n-2}$.

As will be shown below, the "symmetric" bending modes listed in Table 11 are of major importance for concerted tunneling not only because of their high values. Both the "symmetric" bending and the "symmetric" O−O and F−F stretching frequencies listed in Table 12 are very similar for water and hydrogen fluoride cluster transition states.

The imaginary frequencies are listed in Table 13. The reduced masses belonging to the imaginary frequencies are almost equivalent to the one of a single hydrogen atom. This indicates that it is a common misunderstanding that concerted tunneling is unlikely because a "large" number of atoms corresponding to a "large" mass has to be moved.

TABLE 12: "Symmetric" O−O and F−F Stretching Frequencies of Transition States [cm^{-1}]

	MP2	B3LYP
$(H_2O)_3$	741	729
$(H_2O)_4$	624	613
$(H_2O)_5$		512
$(HF)_3$	730 [34]	714
$(HF)_4$	622 [34]	608
$(HF)_5$	524	513

TABLE 13: "Imaginary" Frequencies of Transition States [cm^{-1}] (Corresponding Reduced Masses Are Given in Parentheses [amu])

	MP2	B3LYP
$(H_2O)_3$	1833i (1.0262)	1815i (1.0272)
$(H_2O)_4$	1675i (1.0316)	1651i (1.0324)
$(H_2O)_5$		1617i (1.0365)
$(HF)_3$	1733i [34] (1.0329)	1653i [36] (1.0334)
$(HF)_4$	1498i [34] (1.0385)	1403i [36] (1.0389)
$(HF)_5$	1431i [36] (1.0423)	1318i [36] (1.0426)

3.4. Dynamics. *3.4.1. General.* For investigation of dynamics the extrema on the minimum energy path are far from being sufficient.[57] Ideally, one would like to have an analytic representation of the complete energy hypersurface for the systems under consideration. If such a representation is not available, one tries to describe the most relevant parts of the energy hypersurface as well as possible. Besides the energy extrema, the minimum energy path (MEP) and the region in the vicinity are essential for variationally minimizing recrossing by maximizing the generalized free energy. Additionally, these parts of the energy hypersurface are crucial for estimating small curvature tunneling effects.[55]

The treatment of large curvature tunneling effects due to corner cutting also needs information from the area that cannot be described in terms of an expansion of the potential around the MEP.[55] The region containing the points that lie on significant tunneling paths in the large-curvature case is called the reaction swath.[57]

3.4.2. The Minimum Energy Path. Owing to the excellent agreement between B3LYP and MP2 with respect to the barrier heights and the chosen basis set, we decided to investigate the reaction path for the trimer, tetramer, and pentamer of hydrogen fluoride and for the trimer and tetramer of water with the computationally much less demanding B3LYP method in more detail. For each of these five clusters the minimum energy path for the concerted tunneling was calculated in steps of 0.1 au. The Born−Oppenheimer potential energy along minimum energy paths is displayed in Figure 3.

It is rather easy to show that every physical quantity of a symmetric species has to have zero derivatives with respect to changes that break the symmetry. (In more mathematical terms, every physical quantity has to be an even function if the geometry is changed along a direction that corresponds to an eigenspace of the symmetry operator with an eigenvalue of −1.)

For the present study this has the consequence that not only the energy has zero derivative with respect to the reaction coordinate at the symmetric saddle point but also necessarily all generalized normal mode frequencies. To take advantage of this knowledge, we implemented a cubic spline interpolation for the energy and the frequencies in the POLYRATE[50] program. Cubic splines not only interpolate the data points but leave two external conditions undetermined. Most frequently, these two external conditions are chosen in a way to let the second derivatives at the end points of the interpolation interval vanish (this type of spline is called "natural" splines). In this work, however, these two external conditions were chosen

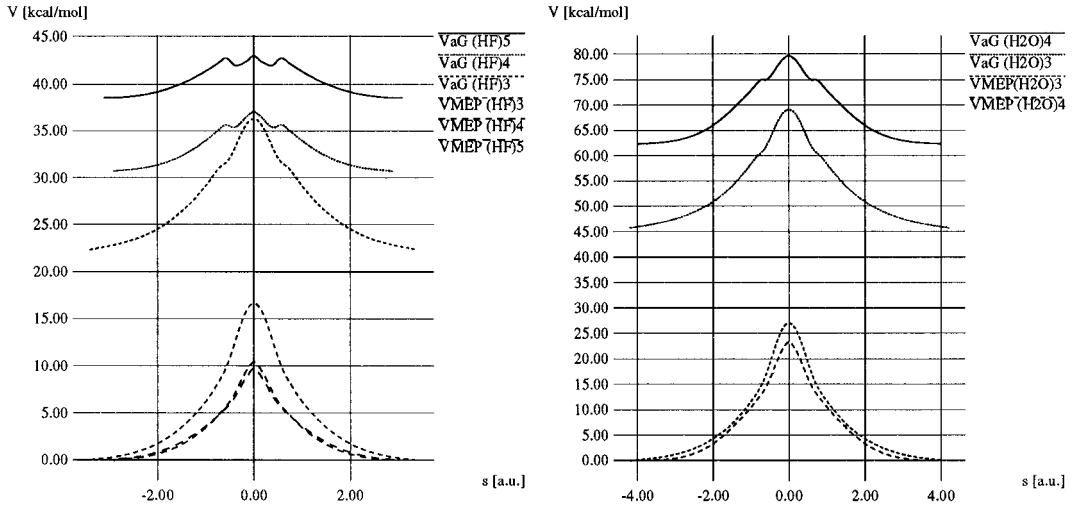

Figure 3. Born−Oppenheimer potential energy (V_{MEP}) and adiabatic ground state potential energy (V_a^G) along the MEP.

differently, i.e., the first derivative vanishes on the saddle point and the second derivative at the minimum of the MEP. This procedure was advantageous with respect to be computational effort required and numerical stability of the calculations, as outlined below.

For the hydrogen fluoride trimer the performance of this strategy was checked by successively calculating energies and generalized normal mode frequencies[70] in steps of $\Delta s = 0.01$ au along the reaction coordinate s between the saddle point and $s = 0.05$ au. These directly calculated generalized normal mode frequencies were compared to the frequencies at these points resulting from fitting generalized normal mode frequencies to points in steps of $\Delta s = 0.1$ au along the minimum energy path. Both methods were found to agree very well. Thus, the chosen procedure helped in avoiding calculations of points very close to the transition state for symmetric reactions. This not only saves computation time but also reduced numerical instabilities that can arise from very small differences between close points on the reaction path.

Starting from the saddle point, the force constant matrix was computed for the pentamer of hydrogen fluoride in steps of 0.1 au along the minimum energy path. The resulting generalized normal modes were reordered by projecting the eigenvectors of successive steps onto each other and connecting the ones giving the largest contribution for a specific eigenvector. As can be seen in Figure 4, the generalized normal mode frequencies mostly change in the range of $s = -1.0$ to $s = +1.0$ of the minimum energy path. Outside this range, changes are less pronounced and easily predictable by interpolation over longer distances. Therefore, for the hydrogen fluoride tetramer the second derivatives were only computed up to $s = 1.4$ and for the hydrogen fluoride trimer up to $s = 1.1$, with an additional point at $s = 2.0$, reordered and connected as described above.

In general the low generalized normal modes increase toward the saddle points, whereas the higher ones decrease. The three most interesting frequencies are the symmetric ones (symmetric H−F stretching, symmetric F−F stretching, and symmetric H−F bending). In all three hydrogen fluoride clusters they show the same characteristic permutation along the minimum energy path. In the beginning the symmetric F−F stretching corresponds to the direction of the reaction path. However, toward the saddle point this mode continuously changes to the H−F stretching. On the saddle point the H−F stretching exactly corresponds to the direction of the minimum energy path. The H−F symmetric bending mode in the minima changes to the symmetric F−F stretching mode on the saddle point (mode 9 for the trimer, mode 12 for the tetramer, and mode 19 for the pentamer of HF in Figure 4; modes are numbered in descending order of the transition state frequencies). The symmetric H−F stretching mode becomes the H−F bending mode, corresponding to the highest frequency of the transition state of the trimer, the second highest of the tetramer, and the third highest of the pentamer (mode 1 for the trimer, mode 2 for the tetramer, and mode 3 for the pentamer of hydrogen fluoride; in the case of the pentamer the highest frequency of the transition state is 2-fold degenerate). For the tetramer and the pentamer of hydrogen fluoride, one "negative" frequency of very small magnitude appears on the reaction path, which is most likely due to numerical inaccuracy in the algorithm for finding the minimum energy path. These are assumed to have no influence on the further considerations.

The trimer and tetramer of water were treated analogously. Owing to stronger coupling of frequencies, especially with modes of hydrogens not taking part in hydrogen bonds, the assignment and meaning of the generalized normal modes are not as clear as in the case of the hydrogen fluoride clusters. For reordering and connecting the frequencies, we relied completely on the projecting procedure described above rather than on trying to mimic the connection scheme of the hydrogen fluoride clusters. The changes of the generalized normal modes along the MEP still show very similar motives.

The consequence for the adiabatic ground state potential energy along the MEP can be seen in Figure 3. Upon the increase of the number of monomers, two characteristic maxima on the left and on the right side of the transition state appear. For the hydrogen fluoride tetramer and pentamer these side maxima are at $s = \pm 0.58$, whereas they show up at $s = \pm 0.69$ for the water tetramer. The appearance of the side maxima is a consequence of a strong increase of higher generalized normal mode frequencies in this region of the reaction path, which is not yet compensated by the lowering of electronic energy toward the minima. However, even for the hydrogen fluoride pentamer the "global" maximum adiabatic ground state potential energy remains at $s = 0$.

Another very important feature for dynamics is the angle change of the reaction coordinate along the minimum energy path[61,71] as displayed in Figure 5. A comparison of the angle change with the study on formic acid dimer[71] reveals some differences. The species investigated in our study display a smaller reaction path curvature near the transition state, especially for the trimer of hydrogen fluoride and the trimer of water. Changing of the angle takes place more rapidly,

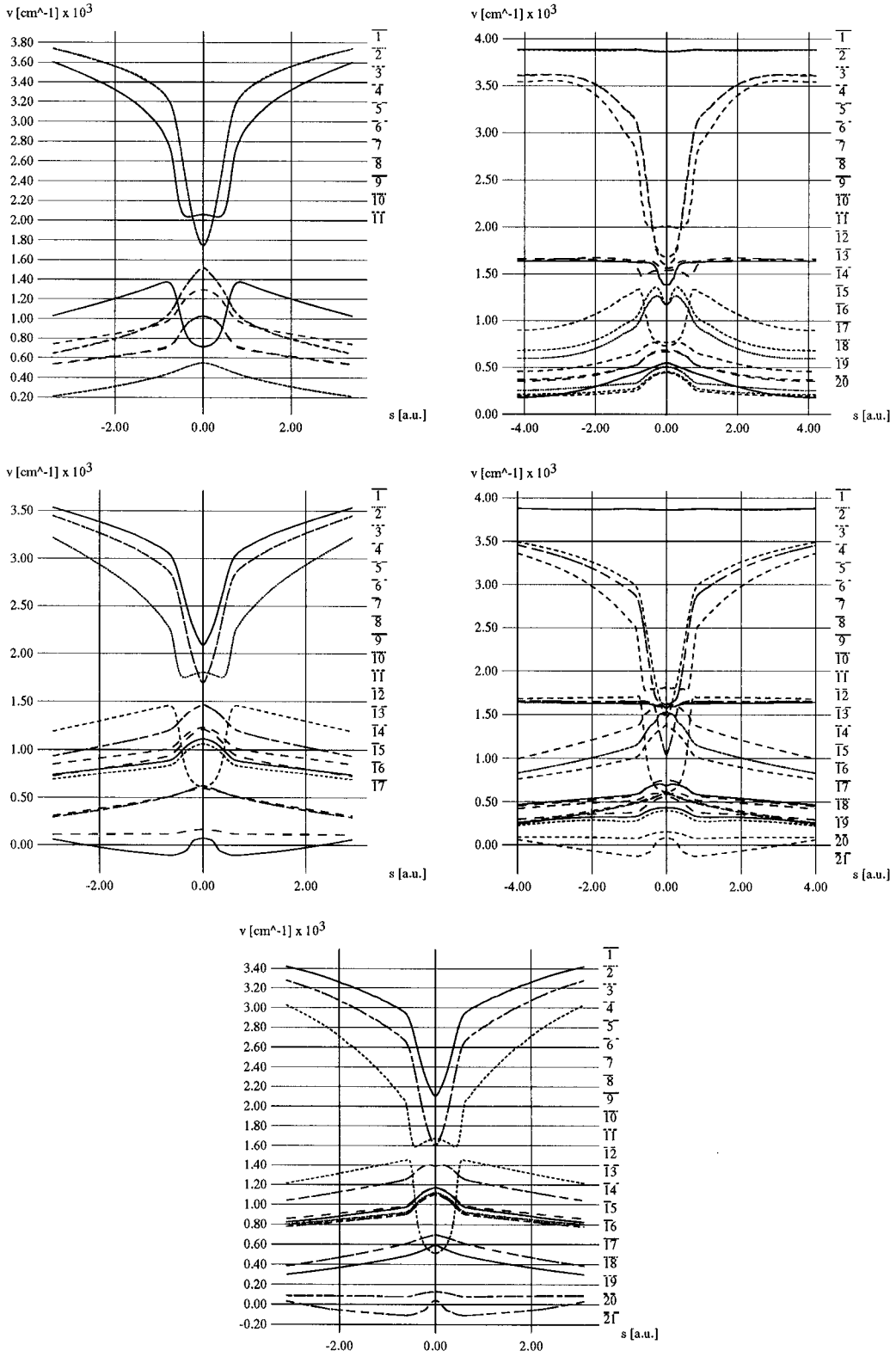

Figure 4. Generalized normal modes along the concerted tunneling MEP of $(HF)_3$ (top left), $(H_2O)_3$ (top right), $(HF)_4$ (middle left), $(H_2O)_4$ (middle right), and $(HF)_5$ (bottom).

indicating that there is nearly an "edge" in the minimum energy path where the reaction coordinate changes from the symmetric H−F stretching mode of the transition state to the symmetric F−F stretching mode of the minimum. This change takes place at the position of the above-discussed side maxima of the adiabatic ground state potential energy on the minimum energy path. In the study of formic acid dimer[71] a similar but less pronounced curvature of the reaction path is apparent, as also can be deduced from the adiabatic ground state potential energy along the MEP. Also, for the formic acid dimer two side maxima appear on the reaction path. Unfortunately, the changes of the generalized normal modes along the minimum energy path are not given for the formic acid dimer and exclude the possibility of a detailed comparison with these results.

3.4.3. Reaction Swath. As mentioned already, the shape and height of the so-called reaction swath determine the relevance of large curvature tunneling because of corner-cutting effects. Owing to the high symmetry of hydrogen fluoride clusters, it

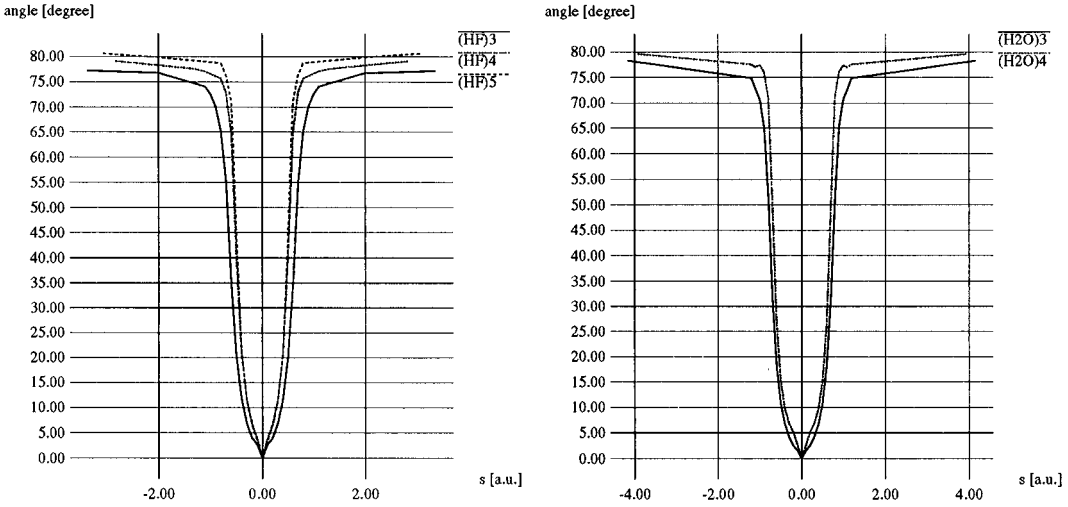

Figure 5. Angle between gradient on the MEP and the "imaginary" mode of the transition states (calculated in steps of 0.1 au and connected).

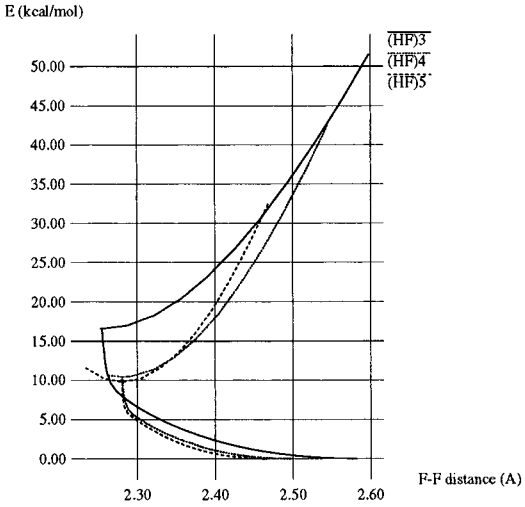

Figure 6. Born−Oppenheimer potential energy on the minimum energy path and on the ridge of the reaction swath for a given F−F distance.

is possible to define the ridge of the reaction swath in a very easy way: One simultaneously has to increase the F−F distance and to force the hydrogens to stay at half angle in between the two fluorine atoms. This corresponds to following the symmetric F−F stretching mode but relaxing the hydrogens' distance from the center of mass. In comparison to the direct following of the symmetric F−F stretching mode of the transition state, this procedure has the advantage that it delivers the lowest hydrogen transition barrier for a given F−F distance but has the disadvantage that the followed direction has, besides the direction of the symmetric F−F stretching mode, contaminations from the symmetric H−F bending mode.

The results of this procedure are shown in Figure 6. Most striking, the ridge is of a rather "harmonic" shape up to the F−F distance of the minima. This implies that the description of the reaction swath by the quadratic approximation is, in contrast to all expectations, at least qualitatively reasonable for nearly the whole region of interest.

3.4.4. Reaction Rates. To get estimates of reaction rates, two different approaches were used. (1) Interpolated variational transition state theory was based on the B3LYP/6-311++G (3df,3pd) description of the minimum energy path and its first and second derivatives. The major disadvantage of this approach is that there is no possiblitiy of including large curvature tunneling effects in the estimate of the reaction rate.[55] This approach will be called B3LYP(SCT) in the following. This B3LYP(SCT) approach was improved by interpolated corrections[65] at the MP2/6-311++G(3df,3pd) level. These corrections include the inertia tensor, the classical barrier height, and all frequencies of the saddle point and minima. This version of the B3LYP(SCT) approach with interpolated corrections will be referred to as MP2///B3LYP(SCT) in the following.

(2) Direct dynamics was used for the trimer of hydrogen fluoride and the trimer of water. This approach was used in order to judge the importance of large curvature tunneling effects that cannot be predicted a priori for unimolecular reactions.[61] Direct dynamics do not rely only on a quadratically approximated surrounding of the minimum energy path but rather calculate the information necessary for large curvature tunneling corrections whenever they are needed. Owing to the large number of calculations that are necessary for such an approach, this method is only feasible at semiempirical level.[57] Whereas AM1[72−76] even fails to reproduce the transition states as first-order saddle points, the description of the reactions with PM3[77,78] is qualitatively right, but classical barrier heights are much too high. The results emerging from this direct dynamics approach with interpolated corrections[65] at the MP2/6-311++G(3df,3pd) level—corrections done exactly as for MP2///B3LYP—will be denoted in the following as MP2///PM3(SCT) for small curvature tunneling corrections and MP2///PM3(LCT) for large curvature tunneling corrections.

The results of all the aforementioned calculations are summarized in Figure 7 showing the reaction rates at 100, 150, 200, 250, and 300 K. In all cases there is no variational effect on the transition state location, i.e., k^{CVT} is identical with k^{TST}. This means that the dynamical bottleneck of each reaction is the saddle point.

In each of the graphs of Figure 7 there are three lines corresponding to successivly more sophisticated methods of tunneling corrections of MP2///B3LYP results. The first curve corresponds to the Wigner method for tunneling corrections. It corresponds to a quadratically approximated one-dimensional barrier assumption. Whereas this is a rather rude estimate, the zero curvature tunneling (ZCT) approximation already takes into account the actual form of the potential along the reactions path. However, this correction still assumes a one-dimensional potential. Finally, the small curvature tunneling (SCT) method—also called centrifugal-dominant small-curvature semiclassical adiabatic ground state (CD-SCSAG) method—not only relies on the actual form of the potential but also includes multidimensional corner-cutting effects on the concave side of

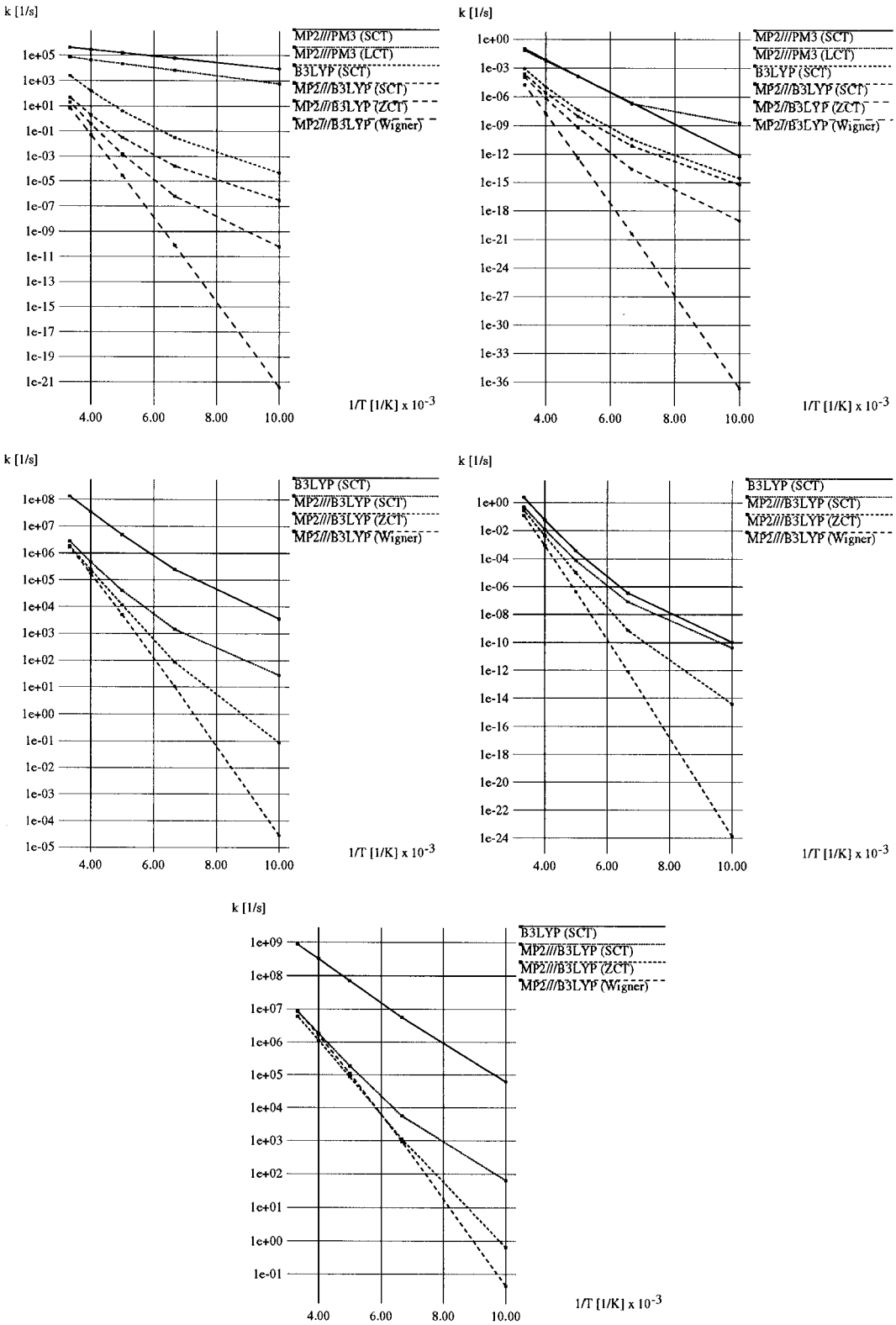

Figure 7. Rate constants of $(HF)_3$ (top left), $(H_2O)_3$ (top right), $(HF)_4$ (middle left), $(H_2O)_4$ (middle right), and $(HF)_5$ (bottom) at the MP2/6-311++G(3df,3pd)///B3LYP/6-311++G(3df,3pd), B3LYP/6-311++G(3df,3pd), and MP2/6-311++G(3df,3pd)///PM3 levels with small curvature tunneling (SCT) and large curvature tunneling (LCT) corrections description.

the reaction path. For low temperatures the difference in the predictions of these three methods range from more than 20 orders of magnitude for the trimer of water to only 3 orders of magnitude for the pentamer of hydrogen fluoride. This indicates that the demands for the proper description of tunneling effects lower with increasing number of monomers. Small curvature tunneling corrections predict enormous tunneling effects in all studied systems as can be seen in Table 14. Owing to the similarity of the reactions under investigation, the small curvature tunneling corrections do not influence the ordering of the reaction rates given by the classical barrier heights.

To give an estimate of the effect of MP2 corrections to the B3LYP calculations, the rate constants directly calculated from B3LYP calculations with small curvature tunneling corrections are shown in Figure 7. The MP2 corrections to B3LYP(SCT) change the calculated rates of the hydrogen fluoride clusters

TABLE 14: Transmission Coefficients from Semiclassical Small Curvature Tunneling Calculations

$\kappa^{SCT}_{MP2///B3LYP}$	100 K	200 K	300 K
$(H_2O)_3$	7.53×10^{22}	2.08×10^{5}	54
$(H_2O)_4$	8.07×10^{14}	1.18×10^{3}	15
$(HF)_3$	2.25×10^{16}	8.24×10^{3}	27
$(HF)_4$	1.99×10^{7}	47	5.2
$(HF)_5$	2.71×10^{4}	9.2	2.9

significantly (up to 3 orders of magnitude), whereas the corrections for the water clusters are comparably smaller (less than 1 order of magnitude). This simply reflects the "better" parametrization of B3LYP and, therefore, the better agreement of B3LYP and MP2 molecular quantum mechanics calculations for water than for hydrogen fluoride.

The MP2///B3LYP(SCT) calculation, due to the careful description of the minimum energy path and its vicinity, should offer a good benchmark for MP2///PM3(SCT) especially because these two calculations are based on the same interpolated corrections. However, the agreement is quite poor. Several reasons could be responsible for such behavior. Above all, the description of the classical barrier height at the semiempirical level is, especially for the hydrogen fluoride clusters, much too high (e.g., 91 kcal/mol for the hydrogen fluoride pentamer). Also, the reproduction of essential parts of the reaction path, where the strongest frequency changes occur, is far from being satisfactory. Furthermore, the structure of the minima at the PM3 level is quite different from the one resulting from ab initio methods. PM3 in particular appears to overemphasize the importance of the symmetric bending mode for the reaction by underestimating the linear character of the hydrogen bonds in the minimum energy structures. Altogether, these deficiencies appear to be responsible for the fact that the rather simple form of representing the hypersurface cannot be regarded as the method of choice.

Nevertheless, it is very interesting that for the trimer of hydrogen fluoride at the MP2///PM3 level, small curvature tunneling is predicted to be more efficient than large curvature tunneling over the whole range of studied temperatures. For the trimer of water the picture changes, but for higher temperatures the small curvature tunneling correction still leads to nearly identical reaction rates as the large curvature correction. At lower temperature, however, the efficiency of large curvature tunneling seems to be higher.

There are mainly two important factors that may influence the further refinement of reaction rates rather strongly. Improved classical barrier heights could easily shift the reaction rates by 2 orders of magnitude. Nevertheless, we think that this effect would be very similar for all clusters, at least within the hydrogen fluoride clusters and within the water clusters. Also, the role of large curvature tunneling is not entirely clear. One way to reduce these problems could be the introduction of more sophisticated interpolated corrections[58] by including additional high level ab initio points that could help in a proper description of the minimum energy path. Reasonable agreement of predictions for small curvature tunneling corrections within, for example MP2///B3LYP and MP2///PM3 is a precondition but not a guarantee for reasonable large curvature tunneling corrections at the MP2///PM3 level.

In addition, the deficiencies of semiemprical calculations could be reduced by specific reaction parameters.[61,79,80] In the process of deriving specific reaction parameters special emphasis should be put on reproducing not only the minimum energy path and the quadratic approximation of the energy surface surrounding it but also on the shape and the height of the reaction swath. A satisfactory reproduction of the minimum energy path alone is not sufficient for a reasonable description of the reaction swath. At least the proper description of the ridge of the reaction swath as displayed in Figure 6, probably including its second derivatives, would be necessary for such a semiempirical description of the energy hypersurface with specific reaction parameters.

4. Conclusions

Despite the fact that the results on the reaction rates in this study can be improved further, some important conclusions can be drawn.

Dynamic electron correlation treatment is essential for the description of concerted proton transfer both in cyclic water and in cyclic hydrogen fluoride clusters. The reaction swath of the concerted proton transfer indicates a reasonable description by harmonic approximation of the energy hypersurface. In the hydrogen fluoride tetramer and pentamer the concerted proton exchange of four and five protons, respectively takes place with reaction rates that are comparable with the concerted exchange rates in carboxylic acid dimers. The large number of simultanously moving protons does not hinder this transfer. Tunneling is very efficient in the concerted proton exchange reaction of all the cyclic hydrogen-bonded clusters under investigation. The concerted proton exchange rates in the studied water clusters are comparably low because of higher exchange barriers. However, it remains unclear how hydrogen bonding of the "free out-of-plane" hydrogens to additional water molecules would affect these transfer processes.

Our calculations also show that hydrogen fluoride clusters are well-suited model systems for studying concerted tunneling in hydrogen-bonded clusters. Even though the concerted hydrogen exchange barriers are considerably higher for water clusters, many common features can be observed. This emphasizes the importance of experimental work on hydrogen fluoride clusters that can provide essential information in a much easier way than is the case for water clusters with their large number of low energy rearrangement possibilities.

For a more accurate refinement of concerted tunneling rates a consideration of large curvature tunneling corrections will be necessary. We think that our results provide a solid basis for further investigations in this direction.

Acknowledgment. The authors are gratefull to Martin A. Suhm and Sotiris S. Xantheas for helpful discussion and comments on the manuscript.

References and Notes

(1) Jeffrey, G. A.; Saenger, W. *Hydrogen Bonding in Biological Structures*; Springer-Verlag: Berlin, 1991.
(2) Bountis, T., Ed. *Proton Transfer in Hydrogen-Bonded Systems*; NATO ASI Series 291; Plenum Press: New York, 1992.
(3) Simkin, B. Y.; Sheikhet, I. I. Proton Transfer Reactions. *Quantum Chemical and Statistical Theory of Solutions*; Ellis Horwood: London, 1995; pp 289−299.
(4) Barnett, R. N.; Landman, U. *J. Phys. Chem.* **1995**, *99*, 17305−17310.
(5) Pomès, R.; Roux, B. *Chem. Phys. Lett.* **1995**, *234*, 416−424.
(6) Xantheas, S. S. *J. Am. Chem. Soc.* **1995**, *117*, 10373−10380.
(7) Siegbahn, P. E. M. *J. Comput. Chem.* **1996**, *17*, 1099−1107.
(8) Tozer, D. J.; Lee, C.; Fitzgerald, G. *J. Chem. Phys.* **1996**, *104*, 5555−5557.
(9) Benderskii, V. A.; Makarov, D. E.; Wight, C. A. Hydrogen Transfer. *Chemical Dynamics at Low Temperatures*; Advances in Chemical Physics LXXXVIII; Wiley: New York, 1994; pp 151−207.
(10) Xantheas, S. S.; Dunning, T. H., Jr. *J. Chem. Phys.* **1993**, *98*, 8037−8040.
(11) Xantheas, S. S.; Dunning, T. H., Jr. *J. Chem. Phys.* **1993**, *99*, 8774−8792.
(12) Xantheas, S. S. *J. Chem. Phys.* **1994**, *100*, 7523−7534.
(13) Xantheas, S. S. *J. Chem. Phys.* **1995**, *102*, 4505−4517.

(14) Liu, K.; Loeser, J. G.; Elrod, M. J.; Host, B. C.; Rzepiela, J. A.; Pugliano, N.; Saykally, R. J. *J. Am. Chem. Soc.* **1994**, *116*, 3507−3512.
(15) Fowler, J. E.; Schaefer, H. F., III. *J. Am. Chem. Soc.* **1995**, *117*, 446−452.
(16) Klopper, W.; Schütz, M. *Chem. Phys. Lett.* **1995**, *237*, 536−544.
(17) Klopper, W.; Schütz, M. *Ber. Bunsen.-Ges. Phys. Chem.* **1995**, *99*, 469−473.
(18) van Duijneveldt-van de Rijdt, J. G. C. M.; van Duijneveldt, F. B. *Chem. Phys.* **1993**, *175*, 271−281.
(19) van Duijneveldt-van de Rijdt, J. G. C. M.; van Duijneveldt, F. B. *Chem. Phys. Lett.* **1995**, *237*, 560−567.
(20) Estrin, D. A.; Paglieri, L.; Corongiu, G.; Clementi, E. *J. Phys. Chem.* **1996**, *100*, 8701−8711.
(21) Pugliano, N.; Saykally, R. J. *Science* **1992**, *257*, 1937−1940.
(22) Garrett, B. C.; Melius, C. F. In *Theoretical and Computational Models for Organic Chemistry*; Formosinho, S. J., et al., Eds.; NATO ASI Series C 339; Kluver Academic: Netherlands, 1991; pp 35−54.
(23) Chalasinski, G.; Cybulski, S. M.; Szczesniak, M. M.; Scheiner, S. *J. Chem. Phys.* **1989**, *91*, 7048−7056.
(24) Quack, M.; Schmitt, U.; Suhm, M. A. *Chem. Phys. Lett.* **1993**, *208*, 446−452.
(25) Quack, M.; Stohner, J.; Suhm, M. A. *J. Mol. Struct.* **1993**, *294*, 33−36.
(26) Karpfen, A.; Yanovitskii, O. *J. Mol. Struct.: THEOCHEM.* **1994**, *307*, 81−97.
(27) Karpfen, A.; Yanovitskii, O. *J. Mol. Struct.: THEOCHEM.* **1994**, *314*, 211−227.
(28) Suhm, M. A.; Nesbitt, D. J. *Chem. Soc. Rev.* **1995**, *24*, 45−54.
(29) Suhm, M. A. *Ber. Bunsen.-Ges. Phys. Chem.* **1995**, *99*, 1159−1167.
(30) Luckhaus, D.; Quack, M.; Schmitt, U.; Suhm, M. A. *Ber. Bunsen.-Ges. Phys. Chem.* **1995**, *99*, 457−468.
(31) Huisken, F.; Kaloudis, M.; Kulcke, A.; Laush, C.; Lisy, J. M. *J. Chem. Phys.* **1995**, *103*, 5366−5377.
(32) Huisken, F.; Tarakanova, E. G.; Vigasin, A. A.; Yukhnevich, G. V. *Chem. Phys. Lett.* **1995**, *245*, 319−325.
(33) Karpfen, A. *Int. J. Quantum Chem. Symp.* **1990**, *24*, 129−140.
(34) Liedl, K. R.; Kroemer, R. T.; Rode, B. M. *Chem. Phys. Lett.* **1995**, *246*, 455−462.
(35) Becke, A. D. *J. Chem. Phys.* **1993**, *98*, 5648−5652.
(36) Märker, C.; Schleyer, P. v. R.; Liedl, K. R.; Ha, T.-K.; Quack, M.; Suhm, M. A. *J. Comput. Chem.*, in press.
(37) Kim, K.; Jordan, K. D. *J. Phys. Chem.* **1994**, *98*, 10089−10094.
(38) Krishnan, R.; Binkley, J. S.; Seeger, R.; Pople, J. A. *J. Chem. Phys.* **1980**, *72*, 650−654.
(39) Frisch, M. J.; Pople, J. A.; Binkley, J. S. *J. Chem. Phys.* **1984**, *80*, 3265−3269.
(40) Gill, P. M. W.; Johnson, B. G.; Pople, J. A.; Frisch, M. J. *Chem. Phys. Lett.* **1992**, *197*, 499−505.
(41) Frisch, M. J.; Trucks, G. W.; Schlegel, H. B.; Gill, P. M. W.; Johnson, B. G.; Robb, M. A.; Cheeseman, J. R.; Keith, T. A.; Petersson, G. A.; Montgomery, J. A.; Raghavachari, K.; Al-Laham, M. A.; Zakrzewski, V. G.; Ortiz, J. V.; Foresman, J. B.; Cioslowski, J.; Stefanov, B. B.; Nanayakkara, A.; Challacombe, M.; Peng, C. Y.; Ayala, P. Y.; Chen, W.; Wong, M. W.; Andres, J. L.; Replogle, E. S.; Gomperts, R.; Martin, R. L.; Fox, D. J.; Binkley, J. S.; Defrees, D. J.; Baker, J.; Steward, J. P.; Head-Gordon, M.; Gonzalez, C.; Pople, J. A. *Gaussian 94*, Revision C.3; Gaussian: Inc., Pittsburgh, PA, 1995.
(42) Dunning, T. H., Jr. *J. Chem. Phys.* **1989**, *90*, 1007−1023.
(43) Kendall, R. A.; Dunning, T. H., Jr.; Harrison, R. J. *J. Chem. Phys.*, **1992**, *96*, 6796−6806.
(44) Woon, D. E.; Dunning, T. H., Jr. *J. Chem. Phys.*, **1995**, *103*, 4572−4585.
(45) Peterson, K. A.; Dunning, T. H. Jr. *J. Chem. Phys.* **1995**, *102*, 2032−2041.
(46) Feyereisen, M. W.; Feller, D.; Dixon, D. A. *J. Phys. Chem.* **1996**, *100*, 2993−2997.
(47) Xantheas, S. S. *J. Chem. Phys.* **1996**, *104*, 8821−8824.
(48) Liedl, K. R.; Xantheas, S. S.; Rode, B. M.; Dunning, T. H., Jr. To be published.
(49) Gonzalez-Lafont, A.; Truong, T. N.; Truhlar, D. G. *J. Chem. Phys.* **1991**, *95*, 8875−8894.
(50) Steckler, R.; Hu, W.-P.; Liu, Y.-P.; Lynch, G. C.; Garrett, B. C.; Isaacson, A. D.; Lu, D.-h.; Melissas, V. S.; Truong, T. N.; Rai, S. N.; Hancock, G. C.; Lauderdale, J. G.; Joseph, T.; Truhlar, D. G. *POLYRATE* Version 6.5; University of Minnesota: Minneapolis, 1995.
(51) Hu, W. P.; Liu, Y. P.; Truhlar, D. G. *J. Chem. Soc., Faraday Trans.* **1994**, *90*, 1715−1725.
(52) Hu, W.-P.; Lynch, G. C.; Liu, Y.-P.; Rossi, I.; Stewart, J. J. P.; Steckler, R.; Garrett, B. C.; Isaacson, A. D.; Lu, D.-h.; Melissas, V. S.; Truhlar, D. G. *MORATE*, Version 6.5; University of Minnesota: Minneapolis, 1995.
(53) Garrett, B. C.; Truhlar, D. G.; Grev, R. S. Determination of the Bottleneck Regions of Potential Energy Surfaces for Atom Transfer Reactions by Variational Transtition State Theory. In *Potential Energy Surfaces and Dynamics Calculations for Chemical Reactions and Molecular Energy Transfer*; Truhlar, D. G., Ed.; Plenum Press: New York and London, 1981; pp 587−637.
(54) Truhlar, D. G.; Garrett, B. C. *Annu. Rev. Phys. Chem.* **1984**, *35*, 159−189.
(55) Truhlar, D. G.; Isaacson, A. D.; Garrett, B. C. Generalized Transition State Theory. In *Theory of Chemical Reaction Dynamics*; Baer, M., Ed.; CRC Press: Boca Raton, FL, 1985; pp 65−137.
(56) Tucker, S. C.; Truhlar, D. G. Dynamical Formulation of Transition State Theory: Variational Transition States and Semiclassical Tunneling In *New Theoretical Concepts for Understanding Organic Reactions*; Bertrán, J., Csizmadia, I. G., Eds.; NATO ASI Series C 267; Kluwer: Dordrecht, The Netherlands, 1989; pp 291−346.
(57) Truhlar, D. G.; Gordon, M. S. *Science* **1990**, *249*, 491−498.
(58) Truhlar, D. G. Direct Dynamics Method for the Calculation of Reaction Rates in *The Reaction Path in Chemistry: Current Approaches and Perspectives*; Heidrich, D., Ed.; Kluwer: Dordrecht, 1995; pp 229−255.
(59) Michael, J. V.; Fisher, J. R. *J. Phys. Chem.* **1990**, *94*, 3318−3323.
(60) Kim, Y.; Truhlar, D. G.; Kreevoy, M. M. *J. Am. Chem. Soc.* **1991**, *113*, 7837−7847.
(61) Liu, Y.-P.; Lynch, G. C.; Truong, T. N.; Lu, D.-h.; Truhlar, D. G.; Garrett, B. C. *J. Am. Chem. Soc.* **1993**, *115*, 2408−2415.
(62) Melissas, V. S.; Truhlar, D. G. *J. Chem. Phys.* **1993**, *99*, 3542−3552.
(63) Melissas, V. S.; Truhlar, D. G. *J. Chem. Phys.* **1993**, *99*, 1013−1027.
(64) Melissas, V. S.; Truhlar, D. G. *J. Phys. Chem.* **1994**, *98*, 875−886.
(65) Corchado, J. C.; Espinosa-Garcia, J.; Hu, W.-P.; Rossi, I.; Truhlar, D. G. *J. Phys. Chem.* **1995**, *99*, 687−694.
(66) Hu, W.-P.; Truhlar, D. G. *J. Am. Chem. Soc.* **1995**, *117*, 10726−10734.
(67) Mielke, S. L.; Lynch, G. C.; Truhlar, D. G.; Schwenke, D. W. *J. Phys. Chem.* **1994**, *98*, 8000−8008.
(68) Truhlar, D. G.; Garrett, B. C.; Klippenstein, S. J. *J. Phys. Chem.* **1996**, *100*, 12771−12800.
(69) Szabo, A.; Ostlund, N. S. Many-Body Perturbation Theory. *Modern Quantum Chemistry*; McGraw-Hill: New York, 1989; 320−379.
(70) Miller, W. H.; Handy, N. C.; Adams, J. E. *J. Chem. Phys.* **1980**, *72*, 99−112.
(71) Kim, Y. *J. Am. Chem. Soc.* **1996**, *118*, 1522−1528.
(72) Dewar, M. J. S.; Thiel, W. *J. Am. Chem. Soc.* **1977**, *99*, 4899−4907.
(73) Dewar, M. J. S.; McKee, M. L.; Rzepa, H. S. *J. Am. Chem. Soc.* **1978**, *100*, 3607.
(74) Davis, L. P.; Guidry, R. M.; Williams, J. R.; Dewar, M. J. S.; Rzepa, H. S. *J. Comput. Chem.* **1981**, *2*, 433−445.
(75) Dewar, M. J. S.; Zoebisch, E. G.; Healy, E. F.; Stewart, J. J. P. *J. Am. Chem. Soc.* **1985**, *107*, 3902−3909.
(76) Dewar, M. J. S.; Reynolds, C. H. *J. Comput. Chem.* **1986**, *7*, 140−143.
(77) Stewart, J. J. P. *J. Comput. Chem.* **1989**, *10*, 209−220.
(78) Stewart, J. J. P. *J. Comput. Chem.* **1989**, *10*, 221−264.
(79) Liu, Y.-P.; Lu, D.-h.; Gonzalez-Lafont, A.; Truhlar, D. G.; Garrett, B. C. *J. Am. Chem. Soc.* **1993**, *115*, 7806−7817.
(80) Gonzalez-Lafont, A.; Truong, T. N.; Truhlar, D. G. *J. Phys. Chem.* **1991**, *95*, 4618−4627.